Collision Analysis of Lunar High-Speed Landing Mechanism and Foam Metal Fracture Under Extreme Temperature

XU Jian[1*], *LI Qiang*[2], *YANG Zhen*[1], *SUN Yucheng*[3], *LI Zhongming*[1,4]

1. School of Mechanical and Electrical Engineering, North University of China, Taiyuan 030051, P.R.China;
2. Institute of Military-Civilian Integration and Innovation, North University of China, Taiyuan 030051, P.R.China;
3. China Academy of Space Technology, Beijing 100081, P.R.China;
4. PERA of China, Beijing 100089, P.R.China

(Received 29 November 2021; revised 29 March 2022; accepted 21 April 2023)

Abstract: The stress and strain of the components composed of prefabricated grooves, warheads, foam titanium, foam aluminum and the detector are calculated when they rush to the moon surface rocks at a speed of 130 m/s and under 1/6 gravity of earth. The foam metal in the component can bear the force of the detector and provide the recoil force. The stress of preformed groove and warhead is 1 200—2 000 MPa, while the stress of foam titanium and foam aluminum is 10 MPa and 1 MPa, respectively, with significant reduction. The stress of foam titanium is reduced to 1%, and that of foam aluminum is reduced to 1 ‰. The component has also undergone a series of different angle collision tests at low temperatures (−182.85 ℃) and high temperatures (127.15 ℃), and the detector can still operate normally.

Key words: space exploration; collision response; extreme temperature; foam metal; impact resistance

CLC number: V41 **Document code:** A **Article ID:** 1005-1120(2023)03-0354-13

0 Introduction

The average distance between the moon and the earth is 384 400 km, about 30 times the diameter of the earth[1-2]. On May 16, 2019, the National Astronomical Observatory of the Chinese Academy of Sciences announced that the research team led by the researcher Li Chunlai used the Chang'e 4 probe data to prove that the olivine and low-calcium pyroxene existed in the antarctic-Aitken basin on the back of the moon[2].

In the United States, the "Ranger" series, and the "Surveyor" series were launched continuously from 1962 to 1968, and the first satellite "Clementine" equipped with a laser altimeter was launched in 1994. European Space Agency (ESA) launched Smart-1 in 2006. Japan launched the "Luna" Selene in 2007[3].

Some remote sensing lunar exploration research has been carried out earlier. The means of these remote sensing lunar explorations mainly include X-ray and γ-ray spectrometers, such as LP, XRS , and GRS of SELENE, multispectral, hyperspectral remote sensing, etc; Lidar remote sensing, such as LOLA of LRO. The multi-spectral data were used to study the iron-iron content inversion model, and the full-time iron-titanium content was successfully inverted. Based on M3 data, it is found that there is water ice in the lunar polar zone, and there is a new type of magnesium-rich spinel rock on the back of the moon. The distribution of pure plagioclase rocks throughout the month was obtained based on MI data. The distribution of uranium elements throughout the month was obtained based on the Moon Goddess GRS data. The SP data were used to study the source of the olivine in the lunar

*Corresponding author, E-mail address: zdp12_0@126.com.

How to cite this article: XU Jian, LI Qiang, YANG Zhen, et al. Collision analysis of lunar high-speed landing mechanism and foam metal fracture under extreme temperature[J]. Transactions of Nanjing University of Aeronautics and Astronautics, 2023, 40(3): 354-366.

http://dx.doi.org/10.16356/j.1005-1120.2023.03.010

impact basin, and some olivines were derived from the upper mantle of the moon[4]. The SP and MI data were used to study the distribution and geological origin of the pebbles in the moon basin. A lunar crater is an annular pit formed by the impact of a meteorite on the surface of a planet, satellite, asteroid, or other celestial body.

We learned that the densities of titanium foam, 30CrMnSiA, aluminum foam, and the detector are 1 280—2 245 kg/m^3, 7 800 kg/m^3, 270—1 000 kg/m^3 and 2 705 kg/m^3, respectively[5].

Due to the lack of air resistance on the moon, the lunar gravity is 1/6 of the earth, the bullet speed is 130±10 m/s, and the angle is $\pi/2$. The model is shown in Fig.1.

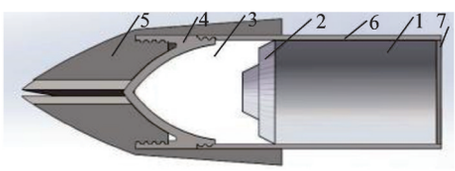

1:Detector 2:Aluminum foam 3:Titanium foam 4:Warhead
5:Prefabricated groove 6:Appearance 7:Detector backpacker

Fig.1 Bullet structure

Each component in the connection is connected separately. The screws are used to connect the warhead and prefabricated groove. They are pressed together and cannot move. Because according to the specification of ANSYS, they should be bonded. When the bullet structure penetrates the moon soil or moon rock, after buffering, the detector will ignite the gunpowder and be driven by the gunpowder. The detector detects the rock and obtains data in the absence of air.

In the high-speed lunar surface collision analysis, when the component hits the rock surface, the component detector will find the data or send the image back.

1 Moon Rock

According to the analysis report of the samples brought back by the former Soviet Union and the United States, the basic composition and formation of the moonstone are not very different from the rocks on the earth[6-7], but there are differences in the distribution, so the drilling is underway.

Rock is a set of one or more minerals under the influence of a complex environment. The physical and mechanical properties of rocks are given in the composition of the mineral particles and the form of the connection. Different connections make the structure of rock different. The causes for the formation can be divided into three types: Magmatic rock, sedimentary rock, and metamorphic rock[7].

Sedimentary rocks are generally rocks formed at shallower places on the surface, weathering products of other rocks and some volcanic eruptions through water flow or glacial handling, sedimentation, and diagenesis. Sedimentary rocks mainly contain particulate matter and cemented matter. Limestone and sandstone belong to sedimentary rocks.

Rock strength[6-7] is a key indicator for judging the mechanical properties of rock, represented by the maximum stress that rock can withstand in the event of impending damage. The uniaxial compressive strength of the rock σ indicates the maximum limit stress that the rock sample can withstand when subjected to axial pressure. It is the ratio of the maximum fracture force F to the cross-sectional area S of the rock specimen, recorded as

$$\sigma = FS^{-1} \tag{1}$$

Many experimental studies have found that the test results of rock specimens with different specifications and surface quality are also different. The smaller the size of the rock sample, the greater the strength of the rock. The more uneven specimens will produce a stress concentration effect, which will reduce the strength of the rock.

According to the uniaxial compressive strength of the rock, the rock is generally classified to five types, as shown in Table 1.

Table 1 Rock types

Rock type	Uniaxial compressive strength/ MPa
Soft	25—50
Hard	50—75
Medium-hard	75—100
Tough	100—200
Hard callous	>200

Rock hardness is a property of rock resisting local deformation or fracture under the action of external force. It can also be regarded as the resistance generated when the rock is invaded by external tools. The relationship between the hardness of the rock and the uniaxial compressive strength of the rock can be approximated as

$$\sigma_k = k\sigma_i \tag{2}$$

where k is given in the type of rock, and its value is generally greater than 1. The grading of the rock drillability is the basis for the development of drilling tools.

The shape and volume change of the rock under the influence of an external force or other physical factors is called deformation. In the microscopic case, the position of the internal mass point will change. Rock denaturation is an important part of rock's mechanical properties. The deformations of rocks[8-9] are divided into elastic deformation, plastic deformation, elastoplastic deformation, etc., according to their failure characteristics. When the rock is subjected to external loads, the elastic and plastic properties can be simultaneously exhibited.

For the brittle rock[10], the pressure is located in a linear relationship with the indentation depth before the failure occurs. When the stress is applicable beyond its damage limitation, it will be violently destroyed. The brittle rock can be used as the elastic object model. Plastic brittle rock, such as marble undergoes elastic deformation before plastic deformation, and then plastic deformation occurs. Finally, brittle failure occurs.

After the rock force reaches the elastic limit, the deformation caused by the intrusion increases, and the force remains unchanged. When the applied external force is very small, the rock can deform plastically without causing brittle failure. This is called unnatural rock.

Therefore, Level 5 is solid muddy shale, unsound sandstone and limestone, and soft gravel. According to Ref.[11], the plastic dynamics model of granite is shown in Table 2.

The values in the material model can generally be found through the material manually, but the elastic modulus of granite is generally from 5 GPa to 66 GPa, so the range of variation is very large and it needs further testing. This model is suitable for rock simulation under large deformation, as shown in Table 3.

Table 2 Material parameters of granite plastic dynamics model[11]

Parameter	Value
Density/(kg•m^{-3})	2 600
Elastic modulus/Pa	0.55×10^{11}
Poisson's ratio	0.27
Tangent modulus/Pa	0
Yield strength/Pa	1.17×10^{8}
Failure strain	0.06

Table 3 Parameters related to moon rock and cutting teeth

Parameter	Moon rock	Carbide cutting teeth
Elasticity/GPa	51.93	600
Poisson's ratio	0.28	0.30
Density/(kg•m^{-3})	2 600	15 000
Coefficient of friction	0.4	0.4

The contact is still carried out in the remaining unit and can be used for the solid unit. As in LS-Dyna[12], it is an eroding model with the *contact_eroding_surface_to_surface. The Lagrangian algorithm is used as the contact surface algorithm. The sliding friction coefficient is 0.4. The other contact is selected as *automatic_nodes_to_surface, the static friction factor is 0.2, and the dynamic friction factor is 0.15.

2 High-Low Temperature Materials

The huge temperature difference on the lunar surface is caused by a combination of factors such as thermal expansion, shrinkage, and fracture of the lunar rock. The high temperature of lunar surface is 400.15 K, and the low temperature is 90.15 K.

The temperature difference between the amplitude causes a large difference in materials, and the material of the structural steel is also related to the temperature. The results of $E, \delta, \psi, \sigma_s, \sigma_b$ also change. E is the modulus of elasticity. δ is the elongation. ψ is the reduction of area. σ_s is the yield

strength, and σ_b is the tensile strength.

The commonly used standards in China's pressure pipeline design[13] are GB50316 "Industrial Metal Pipeline Design Specification", GB/T20801—2006 "Pressure Pipeline Specification Industrial Pipeline", GB50072—2010 "Code for Design of Refrigerator". The tensile strength and yield strength of the test steel tube at low temperatures are both higher than those at room temperature, and the elongation and impact toughness after fracture is reduced.

Mechanical properties at room temperature of experimental steel tubes are shown in Table 4.

Table 5 gives the low-temperature mechanical properties of test steel tubes.

Table 4 Mechanical properties at room temperature of experimental steel tubes

Parameter	Standard value	Actual value
Tensile strength/ MPa	410—530	Vertical:456 Horizontal:487
Yield strength / MPa	＞245	319
Specification of non-proportional extension strength / MPa		333
Rate of elongation after break/ %	20	28.5
Impact energy/ J		19.3

Table 5 Mechanical properties of test steel tubes at low-temperature (243.15 K)

Pipe number	1#	2#	3#	5#
Tensile strength / MPa (Vertical)	560	472	591	542
Yield strength / MPa	403		429	
Specification of non-proportional extension strength / MPa		383		383
Rate of elongation after break / %	26.0	15.7	25.5	
Impact energy /J	18.3		11.8	15.0

In the process of rock cutting and crushing, the displacement field is quasi-continuous, which can be described by the elastoplastic model and calculated by the mechanical theory of the continuous medium. In the continuum theory, rock is considered to be homogeneous and continuous elastoplasticity. When the temperature is too low, brittleness will occur. If the temperature is too high, crystal creep will occur.

Nowadays, the application of the finite element methods in rock mechanics has become more and more extensive, such as the Lagrange grid method, the Euler grid method, the arbitrary Lagrange-Eulerian (ALE) method[11], and the meshless method. Contact between bodies is used, which can transfer force, displacement, etc. LS-Dyna is used for simulation. These objects transfer force and displacement to form stress and strain. When the strain at a certain point is too large and exceeds a certain value, this point will disappear slowly.

The lagrangian grid method is used to establish the finite element model, while the simulation of the martian surface rock mass is combined with the Euler method and the finite element model is established based on the Mohr-Coulomb criterion.

3 High-Speed Landing Plan at Normal Temperature

According to the impact behavior shown in Fig.2, the bullet has a fixed speed, and the rock has a hardness of Level 5, and the bullet attacks the rock vertically.

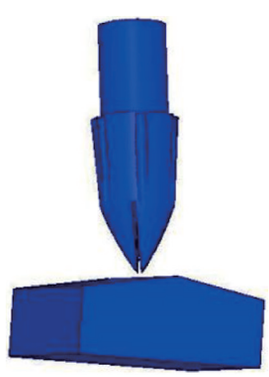

Fig.2 Bullet attacking rock with hardness Level 5

To represent the warhead that touches the rock, the mesh is encrypted here, as shown in Fig.3.

Various materials are still represented by *mat_plastic_kinematic[10] which is used to simulate

Fig.3 Bullet-rock grid

the isotropic hardening. The contact surface between the rock surface and the tip of the prefabricated groove is face-to-face or node-to-face contact, and the node-to-face contact can give a very realistic simulation. This allows the nodes in the prefabricated groove to look for rock surface.

3.1 Prefabricated groove

As the collision is completed, the relevant performances of the prefabricated groove are shown in Figs.4—6.

It can be seen that the stress of the prefabricated groove is 2 100 MPa. Acceleration is about 2 250 m/s^2. But the stress and the acceleration also change inside over time.

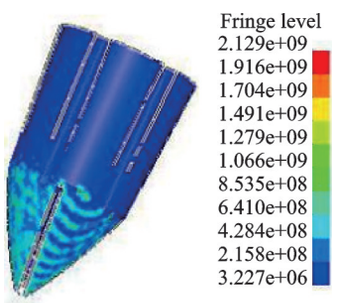

Fig.4 Prefabricated groove stress cloud diagram

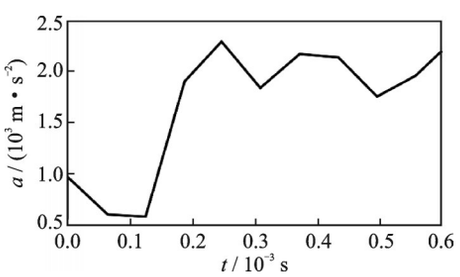

Fig.5 Prefabricated groove acceleration

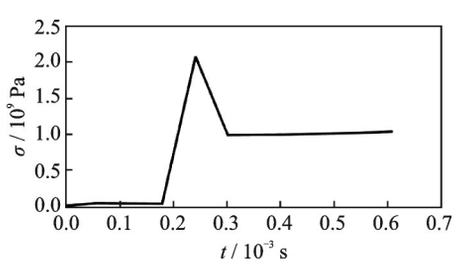

Fig.6 Prefabricated groove stress

3.2 Warhead

As the collision is completed, the relevant performances of the warhead are shown in Figs.7—9.

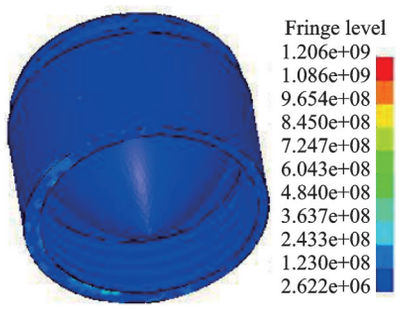

Fig.7 Warhead stress cloud diagram

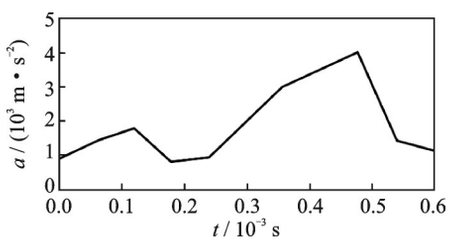

Fig.8 Warhead acceleration

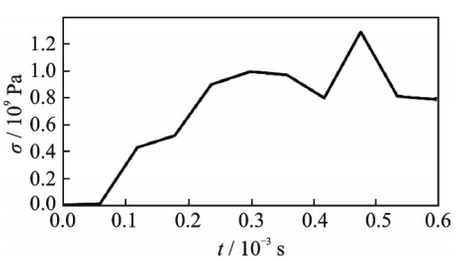

Fig.9 Warhead stress

The maximum stress of the warhead is about 1 200 MPa. The acceleration of the warhead is about 4 000 m/s^2. But the stress and the acceleration also change inside over time.

3.3 Titanium foam

As the collision is completed, the relevant performances of the titanium foam are shown in Figs. 10—12.

The maximum stress of titanium foam can be about 10 MPa. The acceleration of titanium is about 2 500 m/s^2. But the stress and the acceleration also change inside over time.

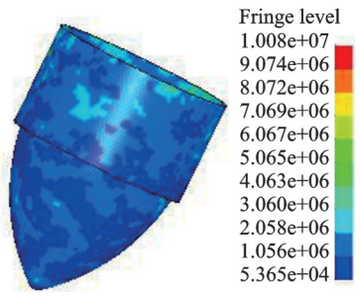

Fig.10 Titanium foam stress cloud diagram

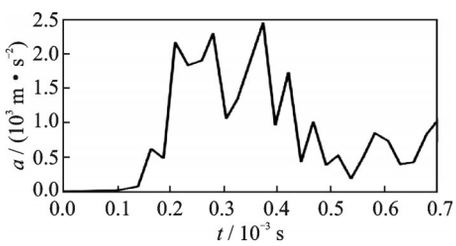

Fig.11 Titanium foam acceleration

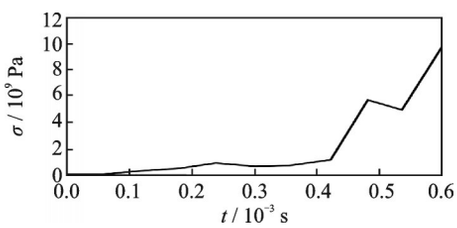

Fig.12 Titanium foam stress

3.4 Aluminum foam

As the collision is completed, the relevant performances of the aluminum foam are shown in Figs.13—15.

It can be seen that the maximum stress of aluminum foam is about 1 MPa. The acceleration of aluminum foam is about 900 m/s^2. But the stress and the acceleration also change inside over time.

Fig.13 Aluminum foam

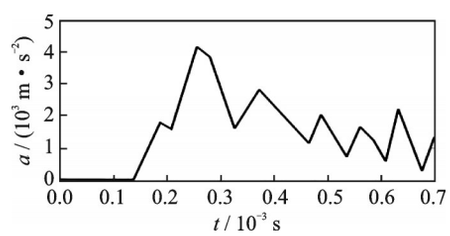

Fig.14 Aluminum foam acceleration

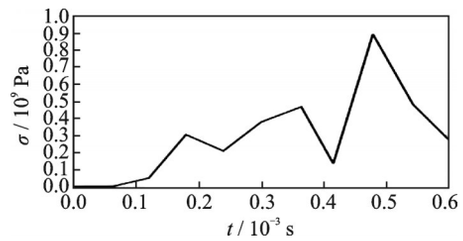

Fig.15 Aluminum foam stress

3.5 Detector

As the collision is completed, the relevant performances of the detector are shown in Figs.16—20.

It can be seen that the stress of the detector is about 30 MPa. The detector acceleration is about 1 800 m/s^2. But the stress and the acceleration also change inside over time. The maximum value is given. The detector is protected by the foam titanium and the foam aluminum, and the stress is reduced a lot.

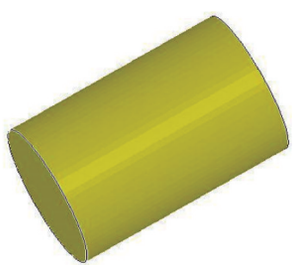

Fig.16 Detector

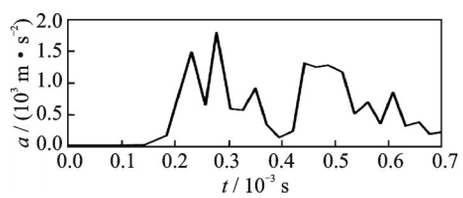

Fig.17 Detector acceleration

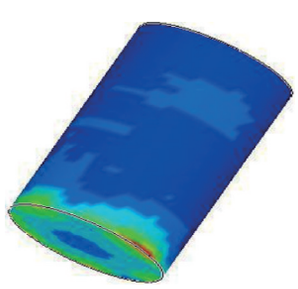

Fig.18 Detector displacement cloud map

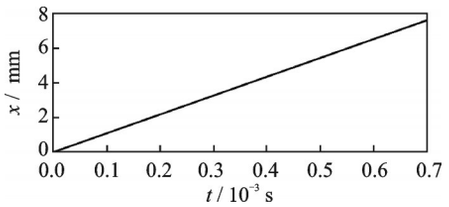

Fig.19 Detector displacement

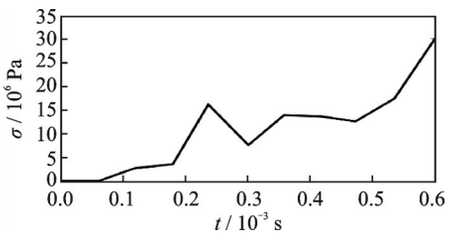

Fig.20 Detector stress

3.6 Appearance

As the collision is completed, the relevant performances of the appearance are shown in Figs.21—23.

Fig.21 Bomb appearance

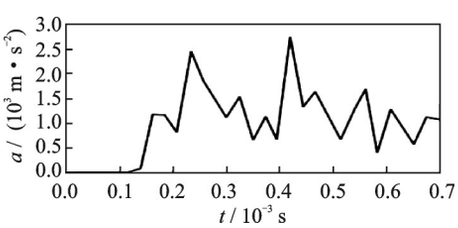

Fig.22 Appearance acceleration of bomb

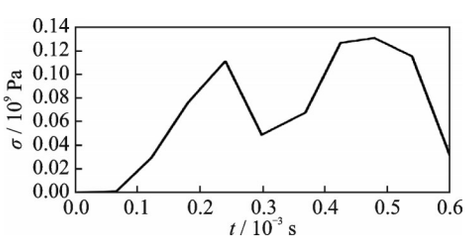

Fig.23 Shell stress of bomb

It can be seen that the maximum stress of the outer casing is about 112.3 MPa. The appearance acceleration is about 2 800 m/s^2. But the stress and the acceleration also change inside over time.

3.7 Detector backpacker

As the collision is completed, the relevant performances of the detector backpacker are shown in Figs.24—26.

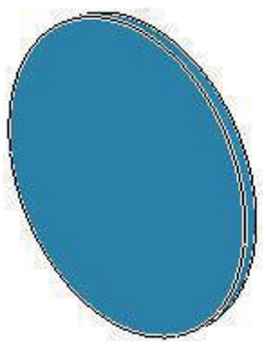

Fig.24 Detector backpacker

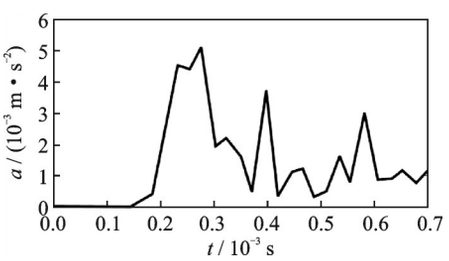

Fig.25 Acceleration of detector backpacker

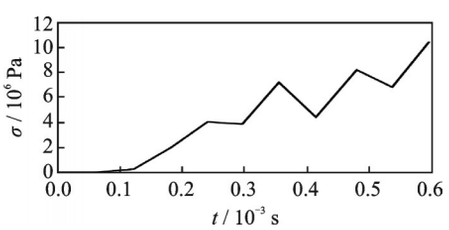

Fig.26 Detector backpacker stress

It can be seen that the maximum stress of the detector backpacker is 11 MPa. The detector backpacker acceleration is about 5 000 m/s^2. But the stress and the acceleration also change inside over time. The maximum value is given in Fig.25 and compared with several other structures, the stress values here are the highest.

3.8 Rock

Some parts of the rock are hit and broken, and the stress is shown in Fig.27. The stress of the rock is also high to 1×10^8 Pa.

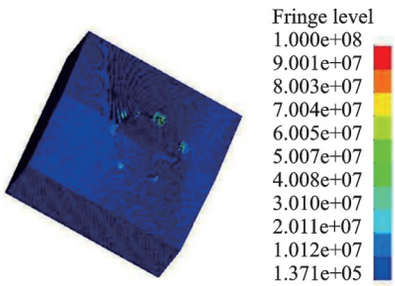

Fig.27 Rock stress cloud diagram

3.9 Analysis of absorption capacity on bullet

The titanium foam and the aluminum foam ensure that the interior of the detector is protected. Unlike prefabricated weakened grooves and warheads, the detector will be damaged once and weaken the stress of the groove and warheads. The stress of 1 200—2 000 MPa of prefabricated groove and warhead is reduced to 10 MPa of foamed titanium which reduces stress by 1%; and 1 MPa of foamed aluminum which reduces stress by 1‰. For the detector, the maximum stress is reduced to 30 MPa.

3.10 Discussion on foam alloys

The porous material is widely used, and it plays a significant role in the structure, cushioning, vibration damping, heat insulation, sound attenuation, filtering, etc. Porous metal is a kind of porous material, while foamed metal is a kind of porous metal. The concept of foamed metal has appeared since the late 1940s. Foam metal is a kind of metal material with a porous structure prepared by special methods.

In general, the following parameters are used to describe the structural characteristics of metal foam[13-17]: Aperture, porosity, apparent density, specific surface area, and through-hole rate.

Different porosity results in different results, as shown in Table 6.

The porosity varies from 50.2% to 71.4%, and the Young's modulus and the yield strength change too much. Therefore, the K file is modified for LS-DYNA calculation. The effect of the porosity of aluminum foam on its mechanical properties is shown in Table 7[18].

Table 6 Mechanical properties of titanium foam

Porosity/%	Yield strength/MPa	Tensile strength/MPa	Young's modulus/GPa
50.2	146.8	193.2	3.3
62.8	48.3	55.6	0.9
71.4	34.4	40.6	0.5

Table 7 Mechanical properties of aluminum foam

Test number item	Porosity/%	E/ MPa	Yield stress/MPa	Energy absorption/(MJ·m^{-3})
1	52	390.8	19.6	9.5
2	58	404	16.2	11.9
3	65	251.1	8.8	10.7
4	73	261.2	7.8	10.0

The stresses of titanium foam and aluminum foam with 71.4% porosity are shown in Fig.28, and the stress reaches 22 MPa. The stress of aluminum foam is not easy to change, which is about 1 MPa in Fig.28.

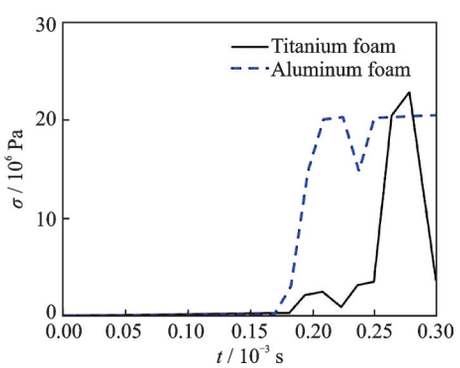

Fig.28 Stress of titanium foam and aluminum foam with 71.4% porosity

The value of the foam aluminum is changed from 71.4% to 52%, and the results are shown in Fig.29. It can be deduced that the properties of alu-

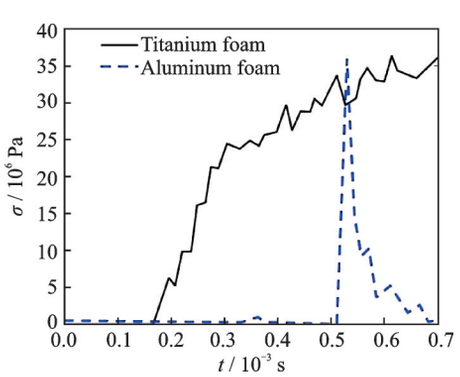

Fig.29 Stress of titanium foam and aluminum foam

minum foam can also make the stresses of titanium and aluminum foam high. The stress of titanium foam is up to 38 MPa, and the stress of aluminum foam is up to 14 MPa.

The elastic modulus of aluminum foam is as small as possible. It brings little impact on the detector. Titanium foam porosity is from 50.2% to 71.4%, and the result is up to 22 MPa.

4 Inclined Collision Analysis

The bullets contact at different angles. Except for $\pi/2$, there are also cases in which the vertical direction are $\pi/6$, $\pi/4$, $\pi/3$, $5\pi/12$ down to the lunar rock. It is possible for a bullet to attack the rock from any angle. Fig.30 shows an example of an attack angle of $\pi/6$.

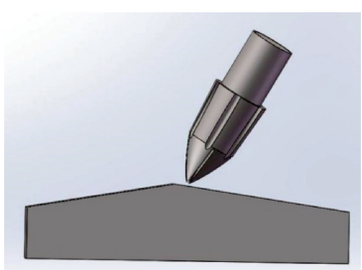

Fig.30 Rock attacking at $\pi/6$

4.1 $\pi/6$ attack on the vertical

According to the rock interpolation, there are no other situations such as rebound when attacking the rock at $\pi/6$, as shown in Figs.31,32.

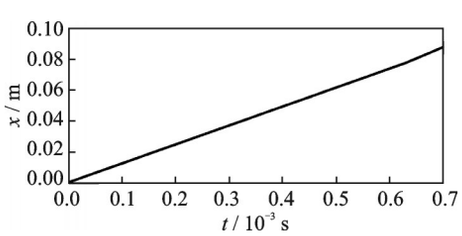

Fig.31 Tip displacement of rock attacking at $\pi/6$

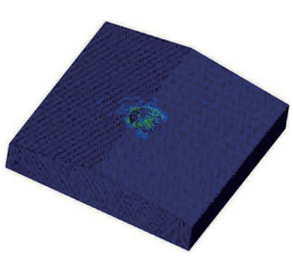

Fig.32 Rupture of rock attacking at $\pi/6$

4.2 $\pi/4$ attack on the vertical

According to the rock interpolation, there are no other situations such as rebound when attacking the rock at $\pi/4$, as shown in Figs.33,34.

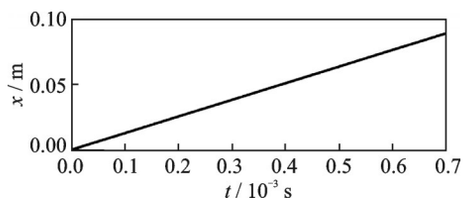

Fig.33 Tip displacement of rock attacking at $\pi/4$

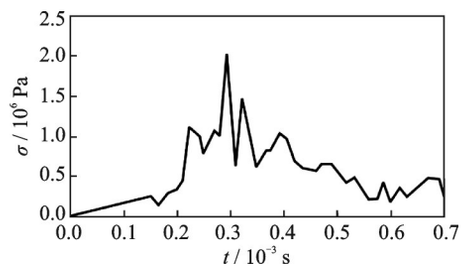

Fig.34 Tip pressure of rock attacking at $\pi/4$

4.3 $\pi/3$ attack on the vertical

According to the rock interpolation, there are no other situations such as rebound when attacking the rock at $\pi/3$, as shown in Figs.35,36

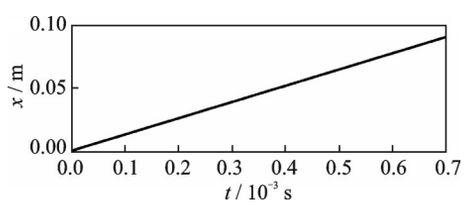

Fig.35 Tip displacement of rock attacking at $\pi/3$

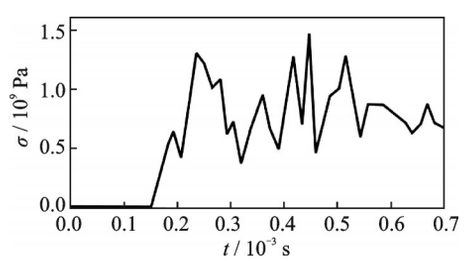

Fig.36 Tip stress of rock attacking at $\pi/3$

4.4 $5\pi/12$ attack on the vertical

According to the rock interpolation, there are no other situations such as rebound when attacking the rock at $5\pi/12$, as shown in Figs.37,38.

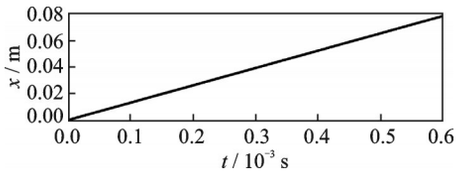

Fig.37 Tip displacement of rock attacking at 5π/12

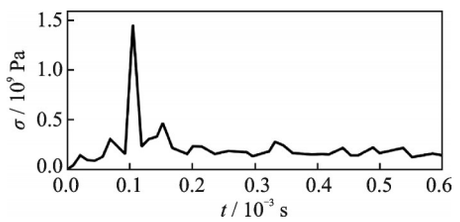

Fig.38 Tip pressure of rock attacking at 5π/12

When the impact object attacks the rock at 5π/12, the rock under the tip of the bullet sticks a little faster, so the stress below is larger.

As the bullet attacks the lunar rock at angles of π/6, π/4, π/3, 5π/12, the attacks should reflect an initial velocity of only 130 m/s plus 1/6 of the earth's gravity on the moon. And the pit body caused by the blow is about 0.08 m, and the intrusion time is about 0.7 ms. The π/3 attack to the vertical is relatively broad, and there is larger stress for a long time. There is no rebound and re-flying into the moon, so it is a case of flying into the moonstone.

5 Extreme Temperature Environment

The bullet mechanical properties are studied when the moon temperature varies from 90.15 K (−182.85 ℃) to 400.15 K(127.15 ℃).

5.1 Hot brittleness in 400.15 K

Elastic modulus E is an important mechanical parameter in material damage and structural safety design. It is used in design and manufacturing and service life assessment.

Under the action of high temperature and short load, the plasticity of the metal material increases. However, after the metal material under the high temperature and long-time load is cooled, the plasticity is significantly reduced, the notch sensitivity is increased, and the brittle fracture phenomenon is often exhibited. This property of metallic materials is called hot brittleness.

With the data in Refs.[12-13], the input K file in this environment is compiled and calculated, and some results are achieved. Stress of the rock and the detector are shown in Figs.39—41.

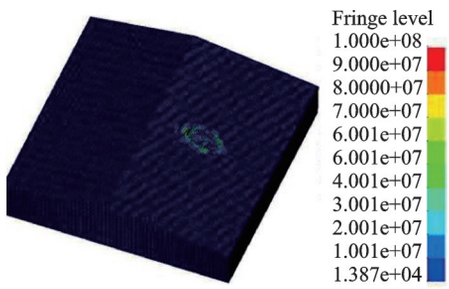

Fig.39 Rock stress at 400.15 K

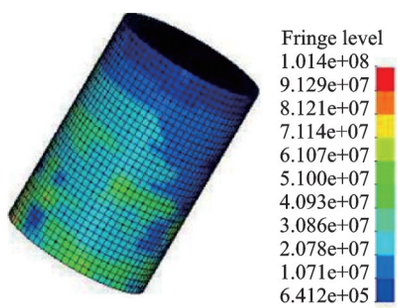

Fig.40 Detector stress at 400.15 K

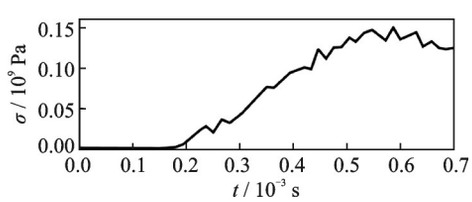

Fig.41 Detector stress-time curve

It can be seen that the stress of the detector is 145 MPa. Generally, being close to the bottom of the detector will bring greater stress.

5.2 Cold brittleness in 90.15 K

As the temperature decreases, the strength of most steel increases and the toughness decreases. The brittleness of metallic materials at low temperatures is called cold brittleness. To prevent low-temperature brittle failure, the minimum allowable operating temperature of the steel should be greater than the upper limit of the ductile-brittle transition temperature.

With the data on some manuscripts, the input

K file is compiled and calculated, and the following results are obtained. The stress of the rock and the detector are shown in Figs.42—44.

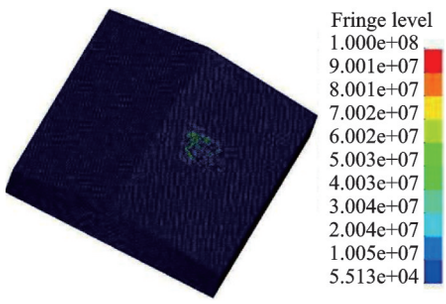

Fig.42 Rock stress at 90.15 K

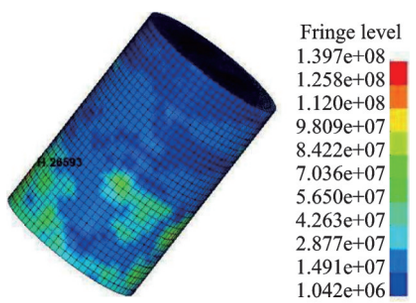

Fig.43 Detector stress at 90.15 K

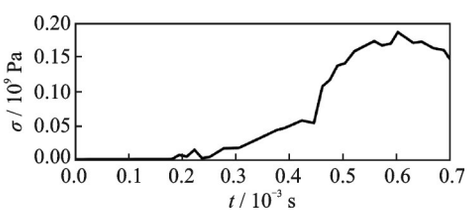

Fig.44 Detector stress-time curve

The detector meets the requirements of both high and low temperatures, and it can be launched in space at any time to obtain scientific data, as shown in Table 8. It can be seen that the stress of the detector is 175 MPa.

Therefore, detectors at high and low temperatures are always at low stress level, which helps to protect the detector. Its stress is always lower than 200 MPa, which helps to protect the detector[18-22].

Table 8 Low-high temperature of detector stress

Temperature/K	Detector stress/MPa
90.15	175
293.15	115
400.15	145

6 Comparison of Experiment and Analytical Data

The experiment is still done on the earth, with a gravity of 9.8 m/s^2. It requires some machines to achieve the moon, gravity of 1/6 of the earth's gravity. With the help of the machine, the experiment is carried out and the stress and acceleration of the groove are measured as shown in Table 9.

Table 9 Acceleration and stress of prefabricated groove

Parameter	Calculated result	Measured result
Stress/MPa	2 100	2 000
Acceleration/(m·s^{-2})	2 250	2 009

The results show that stress and the acceleration are smaller than the values of the calculation. It is good in reality. The prefabricated groove is always broken, just like the calculation result.

7 Others Work

The work of mining rocks on the moon by Baldwin[23] is given in Fig.45. It is similar to the image from OSINSKI's work[24-25], as shown in Fig.46, which is also proved bigger than the one that is tied with a small bullet, but the essence is the same in the low gravity. It could be seen that the moon hit by a smaller bullet still has a cylindrical

Fig.45 Moon rock impact[23]

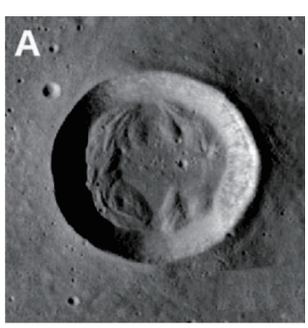

Fig.46 Moon rock impact[24-25]

bottom.

8 Conclusions

The following conclusions are drawn:

(1) The stresses of the prefabricated groove and the warhead are relatively large, which may be 1 200—2 000 MPa. In many cases, it is a process that fails once. Additional components have low stress and can be used once effectively before the groove and warhead failure. It is reduced to 10 MPa of foam titanium and 1 MPa of foam aluminum. The reduction is very large. The basic titanium foam is reduced to 1%, and the aluminum foam is reduced to 1‰. The absorption capacity is very good.

(2)Whether the bullet penetrates the rock vertically or in the direction of $\pi/6$, $\pi/4$, $\pi/3$ and $5\pi/12$ from the vertical line, it can break into the rock and will not rebound and fly into the lunar space.

(3) Given the three temperatures from low to high, the structure is accomplished at an arbitrary temperature. From the analysis, it is possible to carry out the collection work at any time on the moon.

References

[1] JAUMANN R, HIESINGER H, ANAND M, et al. Geology, geochemistry, and geophysics of the moon: Status of current understanding[J]. Planetary and Space Science, 2012, 74(1): 15-41.

[2] CAI Jinman. Chang'e 4 lands at the far side of the moon[J]. Aerospace China, 2018,19(4): 65.

[3] LEMELIN M, LUCEY P G, MILJKOVI K, et al. The compositions of the lunar crust and upper mantle: Spectral analysis of the inner rings of lunar impact basins[J]. Planetary and Space Science, 2019, 165: 230-243.

[4] ASPHAUG E. Impact origin of the Moon?[J]Annual Review of Earth and Planetary Sciences,2014,42(1): 551-578.

[5] SHACKELFORD J F, ALEXANDER W. Materials Science and Engineering Handbook[M]. [S.l.]: CRC Press, 2016.

[6] BORG L E, SHEARER C K, ASMEROM Y, et al. Prolonged KREEP magmatism on the Moon indicated by the youngest dated lunar igneous rock[J]. Nature, 2004, 432(7014): 209-211.

[7] KARATO S I. Geophysical constraints on the water content of the lunar mantle and its implications for the origin of the Moon[J]. Earth Planetary Science Letter, 2013, 384: 144-153.

[8] MELOSH H J, KENDALL J, HORGAN B, et al. South Pole-Aitken basin ejecta reveals the moon's upper mantle[J]. Geology, 2017,45(12): 1063-1066.

[9] TREIMAN A H, KULIS M J, GLAZNER A F. Spinel-anorthosites on the moon: Impact melt origins suggested by enthalpy constraints[J]. American Mineralogist, 2019 ,104(3):370-384.

[10] LI B, LI C, GAO Y M, et al. Influence of heat treatment on corrosion-wear behavior of Ni-based coating in artificial seawater[J]. Journal of Materials Engineering and Performance,2019, 28(12): 7828-7834.

[11] BAI Jinze. LS-DYNA 3D theoretical foundation and experimental analysis[M]. Beijing: Science and Technology Press,2005. (in Chinese)

[12] Livermore Software Technology Corporation.LS-DYNA keyword user's manual[M]. Livermore, California: LSTC, 2015.

[13] WANG L. After service of 20steel under low-temperature mechanical properties research[J]. Refrigeration, 2015, 34(3): 55-60.

[14] WANG M S, QIN Q H, WANG T J. Low-velocity impact and minimum mass design of physically asymmetric sandwich beams with metal foam core[J]. Acta Mechanica, 2015, 226(6): 1839-1859.

[15] XIAO Jian, LIU Jinping, WANG Zhixiang, et al. Structural design of titanium foam[M]. Beijing: Metallurgical Industry Press, 2018: 54-55. (in Chinese)

[16] WANG Lucai, WANG Fang. Perparation, Property and application of foam metal[M]. Beijing: National Defense Industry Press, 2012: 134-135. (in Chinese)

[17] XING Yan, WANG Xiangke. Spacecraft materials [M]. Beijing: Beijing Institute of Technology Press, 2018.

[18] DEGISCHER H-P , KRISZT B. Handbook of cellular metals: Production, processing, applications[M]. [S.l.]: Wiley-VCH Verlag GmbH & Co. KGaA, 2002.

[19] QIU N, GAO Y, FANG J, et al. Crashworthiness analysis and design of multi-cell hexagonal columns under multiple loading cases[J]. Finite Elements Analysis and Design, 2015, 104: 89-101.

[20] BI J, FANG H, WANG Q, et al. Modeling and optimization of foam-filled thin-walled columns for crashworthiness designs[J]. Finite Elements Analysis and Design, 2010,46(90): 698-709.

[21] DEAR J P, LEE H, BROWN S A. Impact damage processes in composite sheet and sandwich honeycomb

materials[J]. International Journal of Impact Engineering, 2005,32(1/2/3/4): 130-154.

[22] PRABOWO A R, BAE D M, CHO J H, et al. Analysis of structural crashworthiness and estimating safety limit accounting for ship collisions on strait territory[J]. Latin American Journal of Solids and Structures. 2017,14(8): 1594-1613.

[23] BALDWIN E C. Investigation of impact crater processes using experimental and numerical techniques [D]. London: University of London, University College London, 2008.

[24] OSINSKI G R, SILBER E A, CLAYTON J, et al. Transitional impact craters on the Moon: Insight into the effect of target lithology on the impact cratering process[J]. Meteoritics & Planetary Science, 2018, 54(3): 64-66.

[25] OSINSKI G R, TORNABENE L L, GRIEVE R A F. Impact eject an emplacement on terrestrial planets[J].Earth Planetary Science Letter, 2011, 310(3/4): 167-181.

Acknowledgements This work was supported by the National Natural Science Foundation of China (No.51175481); the Hubei Sannong Science and Technology Talents Project 2020—2021.

Author Dr. **XU Jian** received the Ph.D. degree from North University of China. He is mainly engaged in the design of friction and lubrication structures.

Author contributions Dr. **XU Jian** calculated the impact process and analyzed the attacking rocks from different angles. Prof. **LI Qiang**, Prof. **YANG Zhen** and Ms. **SUN Yucheng** contributed to the background and method design. Mr. **LI Zhongming** helped with the FEM analysis. All authors commented on the manuscript draft and approved the submission.

Competing interests The authors declare no competing interests.

(Production Editor: SUN Jing)

极端温度下月球高速着陆机构与泡沫金属断裂的碰撞分析

徐 健[1], 李 强[2], 杨 臻[1], 孙玉成[3], 李中明[1,4]

(1.中北大学机电工程学院,太原 030051,中国; 2.中北大学军民融合协同创新研究院,太原 030051,中国; 3.中国空间技术研究院,北京 100081,中国; 4.中国PERA,北京 100089,中国)

摘要:计算了以预制凹槽、弹头、泡沫钛、泡沫铝以及探测器组成的构件以130 m/s的速度,在1/6地球引力下,冲向月球表面岩石所发生的应力应变。构件中的泡沫金属能够承受探测器的力,并提供反冲力。预制凹槽和弹头的应力为1 200~2 000 MPa,而泡沫钛和泡沫铝的应力分别为10 MPa和1 MPa,降低量显著,泡沫钛降低至1%,泡沫铝降低至1‰。该构件还在低温(-182.85 ℃)以及高温(127.15 ℃)下进行了一系列不同的角度碰撞实验,探测器仍可以正常工作。

关键词:太空探索;碰撞响应;极端温度;泡沫金属;抗冲击性